GEOPHYSICS, VOL. 63, NO. 5 (SEPTEMBER-OCTOBER 1998); P. 1767–1778, 9 FIGS.

Asymptotic theory for imaging the attenuation factor *Q*

Alessandra Ribodetti* and Jean Virieux*

ABSTRACT

To describe accurately the propagation of elastic waves for characterizing and monitoring hydrocarbon reservoirs, as well as to obtain improved earth models, it is important to take into account seismic attenuation. We describe a method to estimate anelastic medium properties by a complete SH-waveform inversion. We use an optimization approach based on the iterative minimization of the mismatch between the seismic data and the computed response. To obtain a fast analytical imaging procedure, we include an asymptotic theory for attenuation in a linearized inverse scattering formulation. The forward modeling is solved by the Born approximation for a smooth and attenuative background medium. An asymptotic ray-tracing method is used to calculate traveltime, amplitude, and attenuation between source, receiver, and scattering points. The resulting method is computationally efficient and allows for a variety of data-acquisition geometries, including those with redundant or incomplete source-receiver coverage. Synthetic examples with realistic surface-to-surface geometry show an acceptable convergence in a few iterations when anomaly perturbations are less than 10% of the reference values and when associated diffracting structures are smaller than one-tenth of the predominant seismic wavelength. Through there remains the fundamental trade-off between density and shear modulus, the iterative asymptotic inversion is able to recover the elastic parameters (density and shear modulus) and the attenuation factor.

INTRODUCTION

In seismic exploration, recovering material properties such as attenuation in the subsurface can be as important as recovering the reflectivity of a discontinuity. Reliable estimates of attenuation properties in the earth are significant for improved understanding of lithology, physical state, and the degree of saturation of subsurface rocks. In addition, attenuation propagation may be relevant to the study of "bright spots" in hydrocarbon exploration (Sheriff, 1975).

Many workers have presented algorithms for the reconstruction of elastic parameters from seismic waveforms using different approximations and approaches (Bleistein, 1987; Beydoun and Mendes, 1989; Crase et al., 1990; Beylkin and Burridge, 1990; Jin et al., 1992; Lambaré et al., 1992). However, there have been few investigations of algorithms using the complete seismogram for recovering attenuation properties (e.g. Tarantola, 1988) because this requires consideration of frequency-dependent wave propagation.

We propose here an asymptotic method for imaging the attenuation factor Q using complete waveforms following existing methods developed for the reconstruction of elastic parameters (Jin et al., 1992; Lambaré et al., 1992).

The inverse problem for estimating earth structure from seismic data is currently treated in two different ways. First, using optimization theory, an iterative method can be developed to find a model that best fits the observations within a certain error level. These method are valid for a large variety of source-receiver configurations, but they are computationally expensive (Crase et al., 1990). A second approach, known sometimes as direct inversion, involves the construction of an inverse operator for the forward problem that relates the earth model parameters to the observed seismograms (Bleistein, 1987; Beylkin and Burridge, 1990). This approach is efficient, but it is numerically unstable and allows only specific geometries of data acquisition, such as the zero-offset configuration.

Jin et al. (1992) have introduced a new method for inverting seismic reflection data which follows the optimization approach but which uses specific features of an asymptotic approximation of the forward operator relating parameters and seismograms in order to express the inversion through analytical expressions. This approach is fast and also allows different data acquisition geometries (Lambaré et al., 1992). This method has been extended to diffusive electromagnetic phenomena by Virieux et al. (1994). In this paper, we are concerning with its application to wave propagation in attenuating media (see also Ribodetti et al., 1995).

Manuscript received by the Editor July 2, 1996; revised manuscript received October 1, 1997.
*UMR Géosciences Azur, CNRS-UNSA, site de Sophia Antipolis, Rue A. Einstein, 06560 Valbonne, France. E-mail: ribodeti@faille.unice.fr. E-mail: viri@faille.unice.fr.

Three steps are required for this image reconstruction. (1) In a given, smooth, 3-D reference medium, we build a high-frequency Green's function that depends on traveltime, amplitude, and attenuation factors using an asymptotic ray-tracing method. (2) We express the perturbation of the asymptotic Green's function as a linear integral over the diffracting region containing the model perturbations. We obtain this integral using the first-order Born approximation in the smooth reference medium. (3) We invert asymptotically this linear relation with an analytical estimation of the associated gradient and with an analytical approximation of the corresponding Hessian matrix. Because the attenuation is frequency dependent, the inversion scheme has been developed in the frequency domain.

We test this method on synthetic examples with surface-to-surface geometry. We attempt to recover two thin attenuating layers embedded in a homogeneous viscoelastic medium by inverting synthetic seismograms computed with the reflectivity method (Fuchs and Müller, 1971). We also perform an inversion with noisy data to analyze the robustness of the method. Finally, we evaluate the parameter uncertainties for the recovered model due to uncertainties in the data misfits using the statistical bootstrapping method.

WAVE PROPAGATION AND BORN APPROXIMATION

Modeling anelastic attenuation

As waves propagate through most real materials, the wave amplitudes attenuate as a result of a variety of processes. These processes can be considered macroscopically as "internal friction." The gross effect of internal friction is summarized by the dimensionless quality factor Q, sometimes called intrinsic attenuation or dissipation factor. As an intrinsic property of rock, Q represents the ratio of stored energy to dissipated energy. O'Connel and Budiansky (1978) discussed various definitions of Q and their relationships to the viscoelastic constitutive equations for a given material. Many authors have developed macroscopic stress-strain relations to replace the pure elastic Hooke's law, and hence have obtained equations of motion for materials with a particular dependence of Q on angular frequency ω (Maxwell, 1867; Voigt, 1892; Lomitz, 1957; Müller, 1983; Liu, 1995; for reviews see Lee and Solomon, 1979; Toksöz and Johnston, 1981; Bourbié, 1984).

The attenuative properties of rocks can be estimated by a variety of experiments. For nearly elastic or low-loss, linear solids, a definition of Q may be found through extended stress-strain relations. In these linear, viscoelastic media, the correspondence principle (White, 1965; Eringen, 1980) allows one to replace in the frequency domain the elastic modulus μ by a complex $\hat{\mu} = \mu_R + i\mu_I$ with the following relation:

$$\frac{1}{Q} = \frac{\mu_I}{\mu_R}. \tag{1}$$

In rocks with partially liquid-satured flat cracks, a geological structure that frequently occurs in reservoir environments, the mechanical behavior is similar to a Maxwell body represented by a series of springs and dashpots. Hirono (1935a,b, 1941), Miyabe and Ooi (1948), and Peltier (1974) attempted to explain earth materials with the Maxwell model. For shear-wave propagation, this viscoelastic medium is characterized by a density $\rho(\mathbf{x})$ and a complex shear modulus satisfying

$$\hat{\mu}(\mathbf{x}, \omega) = \mu(\mathbf{x}) + \frac{i}{\omega}\nu(\mathbf{x}), \tag{2}$$

where $\mu(\mathbf{x})$ is the elastic part, the factor $\nu(\mathbf{x})$ is a frequency-independent term related to the attenuation, and ω is the angular frequency. Combining expressions (1) and (2), we can express the quality factor Q as

$$\frac{1}{Q(\mathbf{x}, \omega)} = \frac{\nu(\mathbf{x})}{\mu(\mathbf{x}) \cdot \omega}. \tag{3}$$

For such a body, the Q factor is proportional to the frequency. When the frequency increases, the Q factor increases and, consequently, the attenuation decreases. This dependence in frequency has to be defined before constructing the high-frequency approximation of the propagation. Dependences of Q as a fractional power of the frequency are easily incorporated in our algorithm but require more complicated mechanisms. In this paper, we assume that the frequency bandwidth of the data is sufficiently narrow that deviations by the simple frequency proportionality have only small effects.

We assume that the Q factor incorporates effects that modify locally the amplitude of the wave during propagation.

We write the complex velocity $\hat{c}$ in two parameters, the phase velocity c and the quality factor Q, as proposed by Toksöz and Johnston (1981):

$$\frac{1}{\hat{c}} \to \frac{1}{c}\left(1 + i\frac{\mathrm{sgn}(\omega)}{2Q(\omega)}\right), \tag{4}$$

where the function sgn is 1 for positive argument and -1 for negative argument.

The description of attenuating propagation is best expressed by the density ρ and the complex shear modulus $\hat{\mu}$ when we deal with the Born perturbation theory, though the density ρ, the velocity c, and the quality factor Q represented with the complex velocity $\hat{c}$ are more familiar for rheological description.

Ray theory

We study the propagation of SH-waves with attenuation, and we shall introduce the corresponding high-frequency approximation. This analysis can also be applied to other modes of propagation such as P-to-P, P-to-S, S-to-P, SV-to-SV diffractions; for each case, a specific kernel has to be built. For a source position $\mathbf{s} = (s_1, s_2, s_3)$, let $G(\mathbf{s}, \mathbf{x}, \omega)$ be the scalar displacement field at the point $\mathbf{x}$ which satisfies the linearized equation of motion for isotropic SH propagation,

$$\rho\omega^2 G(\mathbf{s}, \mathbf{x}, \omega) + \nabla \cdot (\mu(\mathbf{x})\nabla) G(\mathbf{s}, \mathbf{x}, \omega) = -\delta(\mathbf{x} - \mathbf{s}). \tag{5}$$

Through the correspondence principle, the attenuation is described by replacing the shear modulus μ with its complex equivalent expression $\hat{\mu}$, giving

$$\rho\omega^2 G(\mathbf{s}, \mathbf{x}, \omega) + \nabla \cdot (\hat{\mu}(\mathbf{x}, \omega)\nabla) G(\mathbf{s}, \mathbf{x}, \omega) = -\delta(\mathbf{x} - \mathbf{s}), \tag{6}$$

to express the propagation with attenuation.

For a smooth, heterogeneous medium, the asymptotic time-harmonic expression for the 3-D Green's function is

$$G_0(\mathbf{s}, \mathbf{x}, \omega) = A_0(\mathbf{s}, \mathbf{x}, \omega)\, e^{i\omega T(\mathbf{s}, \mathbf{x})} \tag{7}$$

for a point source located at $\mathbf{s}$. The traveltime T is given by the integral of slowness along the ray,

$$T(\mathbf{s}, \mathbf{x}) = \int_{\sigma_0(\mathbf{s})}^{\sigma(\mathbf{x})} \sqrt{\rho(\xi)/\mu(\xi)}\, d\xi, \tag{8}$$

where σ is arc length along the ray between the source $\mathbf{s}$ and the point $\mathbf{x}$, and μ is the elastic shear modulus. The amplitude A_0, the first term of the series $\sum_{k=0}^{+\infty} A_k(\mathbf{s},\mathbf{x}, \omega)/(i\omega)^k$, has a frequency dependence related to our selected dependence of the attenuation. The amplitude obtained from the first transport equation (solved in the Appendix A) is

$$A_0(\mathbf{s}, \mathbf{x}, \omega) = \sqrt{\frac{(\rho c J)(\sigma_0(\mathbf{s}))}{(\rho c J)(\sigma(\mathbf{x}))}} |A_0(\sigma_0(\mathbf{s}))| \times e^{-\omega \int_{\sigma_0(\mathbf{s})}^{\sigma(\mathbf{x})} \nu(\xi)/2c(\xi)\mu(\xi)\omega\, d\xi}, \tag{9}$$

where $c = \sqrt{\mu/\rho}$ is the phase velocity, under the low-loss assumption. The first term on the right is the geometrical spreading due to wavefront expansion. The initial value $A_0(\sigma_0(\mathbf{s}))$ is found to be $1/4\pi$ by matching the high-frequency solution and the complete solution for a 3-D homogeneous medium. We recover the amplitude expression for a nonattenuating medium by letting ν go to zero. In a weakly attenuating medium, the attenuation effect results in an exponential decay of the amplitude along the rays as is shown in Figure 1.

The exponentially decaying term, denoted by

$$e^{-\omega \int_{\sigma_0(\mathbf{s})}^{\sigma(\mathbf{x})} \nu(\xi)/2c(\xi)\mu(\xi)\omega\, d\xi} = e^{-\omega \int_{\sigma_0(\mathbf{s})}^{\sigma(\mathbf{x})} (1/2cQ(\omega))(\xi)\, d\xi} = e^{-\omega\alpha(\mathbf{s},\mathbf{x},\omega)},$$

can be interpreted as the imaginary part of a complex traveltime $T + i\alpha$. It represents the attenuation along the raypath between source at $\mathbf{s}$ and the diffracting point at $\mathbf{x}$.

Born approximation

Following the procedure proposed by Beylkin and Burridge (1990) for acoustic and elastic media, we present an extension for a linear, viscoelastic, isotropic, 3-D medium. In our formulation, the complex frequency-dependent terms must be taken into account at each step of the inversion. We assume that the global medium can be separated in two parts: a known, smooth reference medium for which the Green's function may be computed by ray theory and an unknown part representing weak, local perturbation of the reference medium parameters.

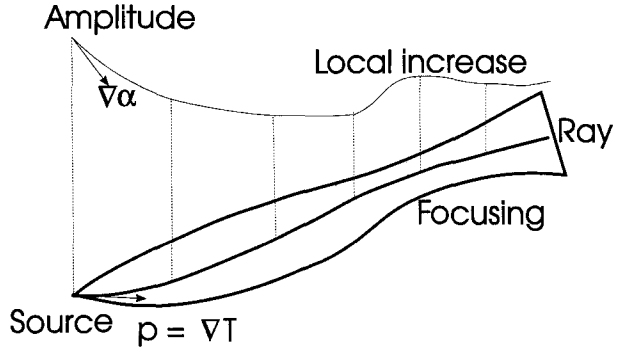

FIG. 1. Ray tracing for an attenuating medium requires supplementary parameters compared to the elastic case, i.e., the vector $\nabla\alpha$ in the direction of maximum spatial attenuation.

The parameters of the global medium can be written as

$$\rho(\mathbf{x}) = \rho_0(\mathbf{x}) + \delta\rho(\mathbf{x})$$
$$\hat{\mu}(\mathbf{x}, \omega) = \hat{\mu}_0(\mathbf{x}, \omega) + \delta\hat{\mu}(\mathbf{x}, \omega), \tag{10}$$

where ρ_0 and $\hat{\mu}_0$ are known background density and shear relaxation function, and $\delta\rho$ and $\delta\hat{\mu}$ are the corresponding first-order perturbations. Both the perturbed and reference media have a frequency-dependent attenuation. Substituting equation (2) into equation (10), we find

$$\hat{\mu}(\mathbf{x}, \omega) = \mu_0(\mathbf{x}) + \delta\mu(\mathbf{x}) + \frac{i}{\omega}(\nu_0(\mathbf{x}) + \delta\nu(\mathbf{x})), \tag{11}$$

in which we distinguish between the elastic (real) and the dissipative (imaginary) terms.

The perturbed Green's function of equation (5) is found using the Born approximation and ray theory. A linear relation over the diffracting domain $\mathcal{M}$ for the leading term in frequency (see Appendix A),

$$\delta G(\mathbf{s}, \mathbf{r}, \omega) = \omega^2 \int_{\mathcal{M}} A_0(\mathbf{s}, \mathbf{x}, \mathbf{r})\, e^{i\omega T(\mathbf{s},\mathbf{x},\mathbf{r})}\, e^{-\omega\alpha(\mathbf{s},\mathbf{x},\mathbf{r},\omega)} \times \underset{\sim}{\mathbf{K}}\underset{\sim}{\mathbf{W}}\mathbf{f}(\mathbf{x})\, d\mathbf{x}, \tag{12}$$

relates perturbation parameters $\mathbf{f}(\mathbf{x}) = (\delta\rho(\mathbf{x}), \delta\mu(\mathbf{x}), \delta\nu(\mathbf{x}))$ to the perturbed Green's function. The kernel $\underset{\sim}{\mathbf{K}}$, combining the effects of different parameters through $(1, 1, i/\omega)$, comes from the specific Maxwell rheology we have assumed. The Ray-Born scattering matrix $\underset{\sim}{\mathbf{W}}$ can be written

$$\begin{pmatrix} 1 & 0 & 0 \\ 0 & \nabla T(\mathbf{s}, \mathbf{x}) \cdot \nabla T(\mathbf{x}, \mathbf{r}) & 0 \\ 0 & \nabla T(\mathbf{s}, \mathbf{x}) \cdot \nabla\tilde{\alpha}(\mathbf{x}, \mathbf{r}) + \nabla\tilde{\alpha}(\mathbf{s}, \mathbf{x}) \cdot \nabla T(\mathbf{x}, \mathbf{r}) & \nabla T(\mathbf{s}, \mathbf{x}) \cdot \nabla T(\mathbf{x}, \mathbf{r}) \end{pmatrix},$$

where $\tilde{\alpha}(\mathbf{s}, \mathbf{x}) = \int_{\sigma(\mathbf{s})}^{\sigma(\mathbf{x})} (\nu_0(\xi)/2c_0(\xi)\mu_0(\xi))\, d\xi$ and $\tilde{\alpha}(\mathbf{x}, \mathbf{r}) = \int_{\sigma(\mathbf{x})}^{\sigma(\mathbf{r})} (\nu_0(\xi)/2c_0(\xi)\mu_0(\xi))\, d\xi$.

The scattering matrix $\underset{\sim}{\mathbf{W}}$ is associated with SH-wave propagation and, for a given position of the scatterer, depends only on the geometry between incident and scattered ray, as shown in Figure 2. For a given position $\mathbf{x}_0$ of the scattering point, the element ∇T is in the direction of phase propagation, i.e., perpendicular to the planes (or surfaces) of constant phase T; the gradient $\nabla\alpha$ is in the direction of maximum spatial attenuation, i.e., perpendicular to the planes (or surfaces) of constant amplitude (Hearn and Krebes, 1990b). The diagonal elements of the scattering matrix involve only the real slowness vector but the other element involves the sum of the scalar products between the slowness $\nabla T(\mathbf{s}, \mathbf{x}_0)$ of the incident ray and the diffracted vector in the direction of maximum spatial attenuation $\nabla\tilde{\alpha}(\mathbf{x}_0, \mathbf{r})$, and between the incident vector in the direction of maximum spatial attenuation $\nabla\tilde{\alpha}(\mathbf{s}, \mathbf{x}_0)$ and the slowness of

the diffracted ray $\nabla T(\mathbf{x}_0, \mathbf{r})$ displayed in Figure 2. The initial value of the attenuation angle can be determined by Fermat's principle (Hearn and Krebes, 1990a).

We may write the linear forward problem (12) in the compact operator form

$$\delta G = \mathcal{G}\mathbf{f}, \tag{13}$$

where $\mathbf{f}(\mathbf{x}) = (\delta\rho(\mathbf{x}), \delta\mu(\mathbf{x}), \delta\nu(\mathbf{x}))$ belongs to the model space $\mathcal{M}$ and δG belongs to the data space $\mathcal{D}$.

ASYMPTOTIC INVERSION THEORY

Inversion by the least-squares method

We obtain the inverse solution of equation (12) through an optimization method where a misfit function between observed and calculated seismograms is minimized. Following the same approach as Jin et al. (1992), we introduce the $\mathcal{L}^2$ least-squares norm misfit function

$$S(\mathbf{f}) = 1/2\langle\delta G^{obs} - \mathcal{G}\mathbf{f}|\delta G^{obs} - \mathcal{G}\mathbf{f}\rangle_{\mathcal{D}} \tag{14}$$

where δG^{obs} are observed data and $\mathcal{G}\mathbf{f}$ are synthetic seismograms estimated through equation (12). The misfit function is defined over the data space by inner product

$$S(\mathbf{f}) = 1/2\sum_{\mathbf{r},\mathbf{s}}\int_{\Omega} d\omega(\delta G^{obs} - \mathcal{G}\mathbf{f})^{\dagger}\mathcal{Q}^{\dagger}\mathcal{Q}(\delta G^{obs} - \mathcal{G}\mathbf{f}), \tag{15}$$

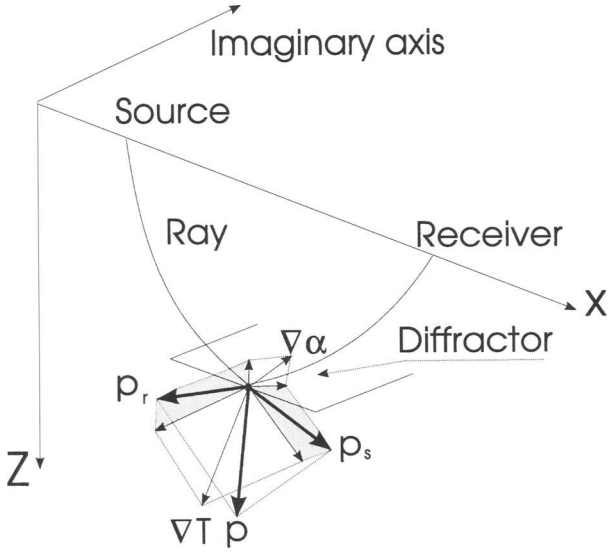

FIG. 2. Diffraction geometry where the source and the receiver are connected through a diffracting point with specific approach angles of rays which control the recovered amplitude of the anomaly. The vector $\nabla\mathbf{T}$ is the gradient of the two-way traveltime and is the sum of the local traveltime of these two rays. The vector $\nabla\boldsymbol{\alpha}$, related to dissipation, is the sum of the vector in the direction of maximal spatial attenuation between the source and the diffracting point and the vector in the direction of maximum spatial attenuation between the diffracting point and the receiver. The slowness vector $\mathbf{p}$ is the sum of $\nabla\mathbf{T}$ and $\nabla\boldsymbol{\alpha}$.

with a weighting matrix $\mathcal{Q}$; the symbol $\dagger$ denotes the complex conjugate. The matrix $\mathcal{Q}$ is the covariance matrix of the stochastic inversion (Tarantola, 1986) and is constructed such that the first iteration of the inversion provides an approximate inverse solution. As proposed by Jin et al. (1992), at the point $\mathbf{x}_0$ of the diffracted region $\mathcal{M}$ where we want to recover model values, the matrix $\mathcal{Q}$ has the form

$$\mathcal{Q} = \begin{pmatrix} \mathcal{Q}_{\rho_0\rho_0} & 0 & 0 \\ 0 & \mathcal{Q}_{\mu_0\mu_0} & 0 \\ 0 & 0 & \mathcal{Q}_{\nu_0\nu_0} \end{pmatrix}, \tag{16}$$

where the terms are defined with ray quantities by

$$\begin{aligned}
&\mathcal{Q}_{\rho_0\rho_0}(\mathbf{s}, \mathbf{x}_0, \mathbf{r}, \omega) \\
&\quad = \frac{|\mathbf{p}(\mathbf{s}, \mathbf{x}_0, \mathbf{r})|}{2\pi\sqrt{2\pi}\omega\, e^{-2\alpha(\mathbf{s},\mathbf{x}_0,\mathbf{r})\omega} A_0(\mathbf{s}, \mathbf{x}_0, \mathbf{r})}\sqrt{Jac} \\
&\mathcal{Q}_{\mu_0\mu_0}(\mathbf{s}, \mathbf{x}_0, \mathbf{r}, \omega) \\
&\quad = \frac{|\mathbf{p}(\mathbf{s}, \mathbf{x}_0, \mathbf{r})|}{2\pi\sqrt{2\pi}\omega\, e^{-2\alpha(\mathbf{s},\mathbf{x}_0,\mathbf{r})\omega} A_0(\mathbf{s}, \mathbf{x}_0, \mathbf{r})}\sqrt{Jac} \\
&\mathcal{Q}_{\nu_0\nu_0}(\mathbf{s}, \mathbf{x}_0, \mathbf{r}, \omega) \\
&\quad = \frac{\omega|\mathbf{p}(\mathbf{s}, \mathbf{x}_0, \mathbf{r})|}{2\pi\sqrt{2\pi i}\omega\, e^{-2\alpha(\mathbf{s},\mathbf{x}_0,\mathbf{r})\omega} A_0(\mathbf{s}, \mathbf{x}_0, \mathbf{r})}\sqrt{Jac},
\end{aligned} \tag{17}$$

where $\mathbf{p}(\mathbf{s}, \mathbf{x}_0, \mathbf{r})$ is the slowness vector and $\sqrt{Jac}$ is the Jacobian that relates the source and station positions at the free surface to properties of the local geometry at the diffracting point $\mathbf{x}_0$ (Jin et al., 1992; Lambaré et al., 1992). We note that the preconditioning associated to the matrix $\mathcal{Q}$ varies with the current position $\mathbf{x}_0$ of the diffracted region; this is an unconventional way to introduce preconditioning. The particular form of the covariance matrix $\mathcal{Q}$ corrects for geometrical spreading and ray obliquity, as well as for the spectral contents of the viscoelastic Green's function. The incorporation of viscoelastic terms in this matrix is a new result. We remark that $\mathcal{Q}_{\nu_0\nu_0}$ is also designed to correct for the frequency dependence of the medium rheology.

Gradient estimation and Hessian approximation

Inversion is obtained by minimizing the misfit function. The expression of the solution $\mathbf{f}$ minimizing the misfit function is well known:

$$\mathcal{G}^{\dagger}\mathcal{G}\mathbf{f} = \mathcal{G}^{\dagger}\delta G^{obs}, \tag{18}$$

where $\mathcal{G}^{\dagger}$ is the adjoint operator of the Ray-Born operator obtained in equation (12). The adjoint operator applied to the observed data, $\mathcal{G}^{\dagger}\delta G^{obs}$, is the gradient of the misfit function, and the term $\mathcal{G}^{\dagger}\mathcal{G}$ is the Hessian. Using the "duality" between the model space and the data space, we construct the kernel $\mathcal{K}$

of this adjoint operator $\mathcal{G}^\dagger$ through the integral definition

$$\mathcal{G}^\dagger \delta G^{obs} = -\sum_{\mathbf{s},\mathbf{r}} \int_\Omega d\omega K^\dagger(\mathbf{s},\mathbf{x},\mathbf{r},\omega)\delta G^{obs}(\mathbf{s},\mathbf{r},\omega), \tag{19}$$

where the inner kernel is expressed as

$$K^\dagger(\mathbf{s},\mathbf{x},\mathbf{r},\omega) = \underset{\sim}{\mathbf{W}}^\dagger \mathcal{Q}^\dagger(\mathbf{s},\mathbf{x}_0,\mathbf{r},\omega)\mathcal{Q}(\mathbf{s},\mathbf{x}_0,\mathbf{r},\omega)$$
$$\times \underset{\sim}{\mathbf{K}}^\dagger A_0(\mathbf{s},\mathbf{x},\mathbf{r})\omega^2 e^{-i\omega T(\mathbf{s},\mathbf{x},\mathbf{r})} e^{-\omega\alpha(\mathbf{s},\mathbf{x},\mathbf{r},\omega)}.$$

The matrices $\underset{\sim}{\mathbf{W}}^\dagger$ and $\underset{\sim}{\mathbf{K}}^\dagger$ are the transposition of $\underset{\sim}{\mathbf{W}}$ and the complex conjugate of $\underset{\sim}{\mathbf{K}}$, respectively.

This last definition of operators is needed for the gradient definition and the Hessian reconstruction associated with the linear system (18).

Following the same approach proposed by Jin et al. (1992), we find that the formal inverse in equation (18) at the diffracting point $\mathbf{x}_0$ can be written as

$$\mathbf{f}(\mathbf{x}_0) = \begin{bmatrix} \delta\rho(\mathbf{x}_0) \\ \delta\mu(\mathbf{x}_0) \\ \delta\nu(\mathbf{x}_0) \end{bmatrix} = \underset{\sim}{\mathbf{H}}^{-1}(\mathbf{x}_0,\mathbf{x})\gamma^0(\mathbf{x}), \tag{20}$$

with an explicit expression of the gradient γ^0 by equation (19) at the point $\mathbf{x}$

$$\begin{bmatrix} \gamma^0_{\rho_0}(\mathbf{x}) \\ \gamma^0_{\mu_0}(\mathbf{x}) \\ \gamma^0_{\nu_0}(\mathbf{x}) \end{bmatrix} = -\sum_{\mathbf{s},\mathbf{r}} \frac{1}{8\pi^3} \int_\Omega d\omega \frac{A_0(\mathbf{s},\mathbf{x},\mathbf{r})}{A_0^2(\mathbf{s},\mathbf{x}_0,\mathbf{r})} Jac$$
$$\times |\mathbf{P}(\mathbf{s},\mathbf{x}_0,\mathbf{r})|^2 e^{-i\omega T(\mathbf{s},\mathbf{x},\mathbf{r})} e^{\omega\alpha(\mathbf{s},\mathbf{x},\mathbf{r},\omega)}$$
$$\times \underset{\sim}{\mathbf{W}}^\dagger \begin{pmatrix} 1 \\ 1 \\ -i\omega \end{pmatrix} \delta G^{obs}(\mathbf{s},\mathbf{r},\omega). \tag{21}$$

The operator $\underset{\sim}{\mathbf{H}}^{-1}$ in equation (20) is the formal inverse of

$$\underset{\sim}{\mathbf{H}} = \mathcal{G}^\dagger\mathcal{G} = \frac{\partial^2 S}{\partial \mathbf{f}^2}, \tag{22}$$

where the function S is the misfit function over frequency. The inverse of the Hessian cannot be calculated analytically. Observing that the diagonal terms are dominant, we obtain a Hessian approximated by

$$\underset{\sim}{\mathbf{H}}(\mathbf{x},\mathbf{x}_0) \sim M_{\mathbf{sr}} \underset{\sim}{\mathbf{W}}^\dagger \underset{\sim}{\mathbf{W}} \cdot \delta(\mathbf{x}-\mathbf{x}_0), \tag{23}$$

where, for a discrete distribution of sources and receivers, Jin et al. (1992) and Lambaré et al. (1992) found that equation (23) must be normalized by $M_{\mathbf{sr}} = 0.5N_\mathbf{s}/\Delta\mathbf{r}$, where $N_\mathbf{s}$ is the number of sources and $\Delta\mathbf{r}$ is the interval between receivers when they are regularly spaced.

For a standard description of the medium rheology, it is possible to recover the global velocity c and the global quality factor Q according to

$$\mathbf{f}'(\mathbf{x}_0) = \begin{bmatrix} c(\mathbf{x}_0) \\ Q(\mathbf{x}_0,\omega) \end{bmatrix} = \begin{bmatrix} c_0(\mathbf{x}_0) + \delta c(\mathbf{x}_0) \\ Q_0(\mathbf{x}_0,\omega) + \delta Q(\mathbf{x}_0,\omega) \end{bmatrix}, \tag{24}$$

where

$$c_0(\mathbf{x}_0) = \sqrt{\mu_0(\mathbf{x}_0)/\rho_0(\mathbf{x}_0)} \quad \text{and}$$
$$Q_0(\mathbf{x}_0,\omega) = \omega \cdot \mu_0(\mathbf{x}_0)/\nu_0(\mathbf{x}_0) \tag{25}$$

are the background quantities and δc and δQ indicate the perturbations of the velocity and the quality factor following the relationship:

$$\delta c(\mathbf{x}_0) = \frac{1}{2}\sqrt{\frac{\rho_0(\mathbf{x}_0)}{\mu_0(\mathbf{x}_0)}}\left[\frac{\delta\mu(\mathbf{x}_0)}{\rho_0(\mathbf{x}_0)} - \frac{\mu_0(\mathbf{x}_0)\delta\rho(\mathbf{x}_0)}{\rho_0^2(\mathbf{x}_0)}\right]$$
$$\delta Q(\mathbf{x}_0,\omega) = \omega\left[\frac{\delta\mu(\mathbf{x}_0)}{\nu_0(\mathbf{x}_0)} - \frac{\mu_0(\mathbf{x}_0)\delta\nu(\mathbf{x}_0)}{\nu_0^2(\mathbf{x}_0)}\right], \tag{26}$$

recovered in each point $\mathbf{x}_0$ of the diffracted domain $\mathcal{M}$.

Because the Hessian expression in equation (23) is only an approximation, we proceed by an iterative quasi-Newtonian approach (Jin et al., 1992) for converging to the best-fitting solution.

For elastic media, the first iteration mimics the solution proposed by Beylkin (1985) and Beylkin and Burridge (1990) for the asymptotic inversion of seismic data. The quasi-Newtonian iteration helps to mitigate some of the errors in the gradient and Hessian estimation and errors due to irregular, arbitrary distributions of sources and receivers.

ILLUSTRATIVE EXAMPLES

Validation of the method

To test our inversion approach, we constructed synthetic seismograms for two thin layers of attenuating material embedded in a homogeneous viscoelastic background medium (Figure 3). The first layer is at a depth of 2000 m and the second at 2500 m; the thickness of each layer is 200 m. A line of receivers is located at the free surface in one direction from an impulsive source at the origin. Since the medium varies in depth only, it is unnecessary to collect data for a true 3-D data aquisition geometry. Stations are spread over 2900 m, which is a realistic configuration because the deepest thin layer is located at 2700 m below the surface; the station spacing is 100 m. The frequency content ranges from 0.2 to 50 Hz. Synthetic seismograms are generated by the reflectivity method (Fuchs and Müller, 1971).

We performed an inversion using two iterations and found the heterogeneities shown in Figure 4. We have recovered the perturbations of the medium parameters (i.e., density, shear modulus, and dissipative factor variations). Because we are looking for a stratified medium, we assume that the experiment

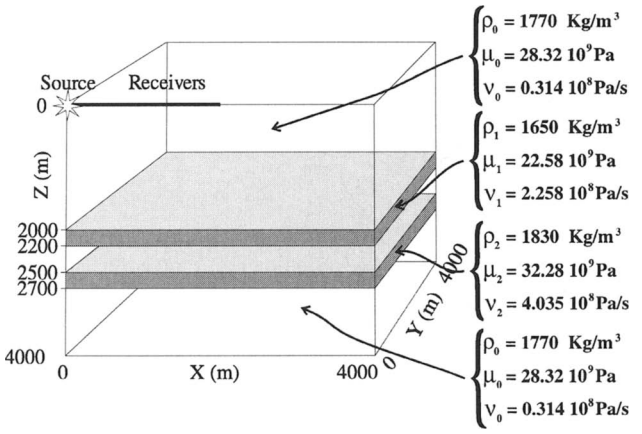

FIG. 3. Two thin attenuating layers are embedded in a homogeneous background medium. The parameters of each layer are plotted on the right. Equivalently, $c_0 = 4000$ m/s, $c_1 = 3700$ m/s, and $c_2 = 4200$ m/s; $Q_0 = \omega\mu_0/\nu_0$, $Q_1 = \omega\mu_1/\nu_1$, and $Q_2 = \omega\mu_2/\nu_2$.

may be repeated for any source translated along the horizontal axis. The image at a given depth is, consequently, the summation of the perturbations recovered at each horizontal distance. This stack results in a recovered medium that is stratified, whereas for only a single source, "diffraction smiles" would have occurred. The main feature is the detection by our inversion technique of layers with similar amplitudes as the input model. The spatial low-frequency component is not well recovered because the layers are rather thin. The trade-off between density and shear modulus is apparent with the slow decay towards the free surface of associated anomalies (Gibbs' effects): their effects cancel each other. Finally the attenuation parameter is well reconstructed near the top boundary, but the quality of the reconstruction deteriorates towards the deepest interface.

In spite of this, we found a good model amplitude fit, which leads us to believe that the inversion algorithm allows recovering of propagation and attenuation parameters.

Using expression (24), we obtain the velocity and the quality factor for the recovered medium. In Figure 5, we note a good

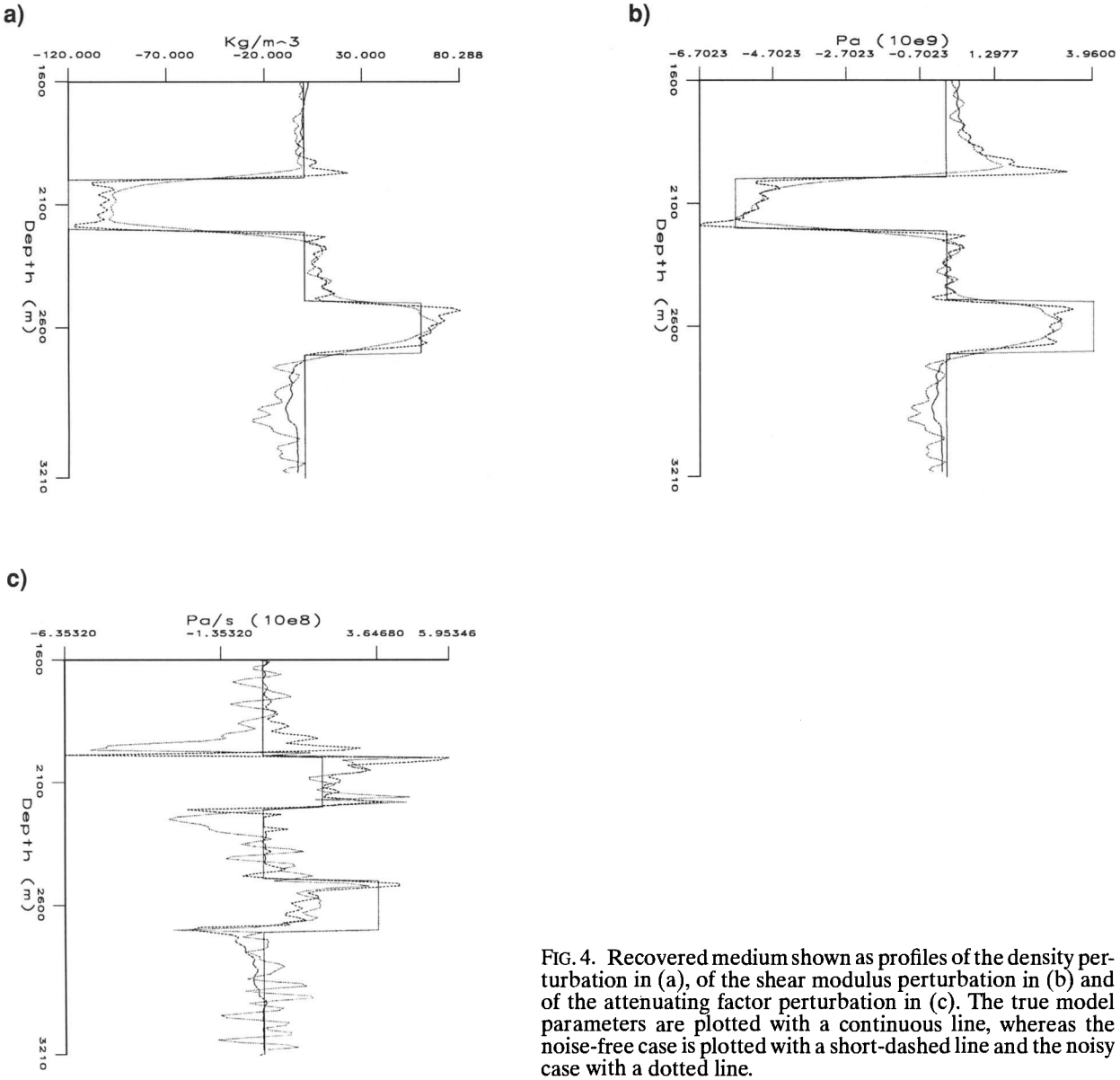

FIG. 4. Recovered medium shown as profiles of the density perturbation in (a), of the shear modulus perturbation in (b) and of the attenuating factor perturbation in (c). The true model parameters are plotted with a continuous line, whereas the noise-free case is plotted with a short-dashed line and the noisy case with a dotted line.

convergence for the velocity parameter: the first anomaly near the interface is balanced by the second anomaly near the second interface. The recovered quality factor is oscillatory due to the frequency dependence of this parameter and the large magnitude of the attenuation variations: the background medium has $Q_0 = \omega\mu_0/v_0$, whereas the first thin layer has $Q_1 = \omega\mu_1/v_1$ and the second one has $Q_2 = \omega\mu_2/v_2$. In any case, a good location of both interfaces is obtained.

To check the convergence of the inversion, we plotted the seismograms in Figure 6. The input seismograms are nearly identical to the inverted seismograms except at the later times; this misfit is associated with the blurring of the recovered image.

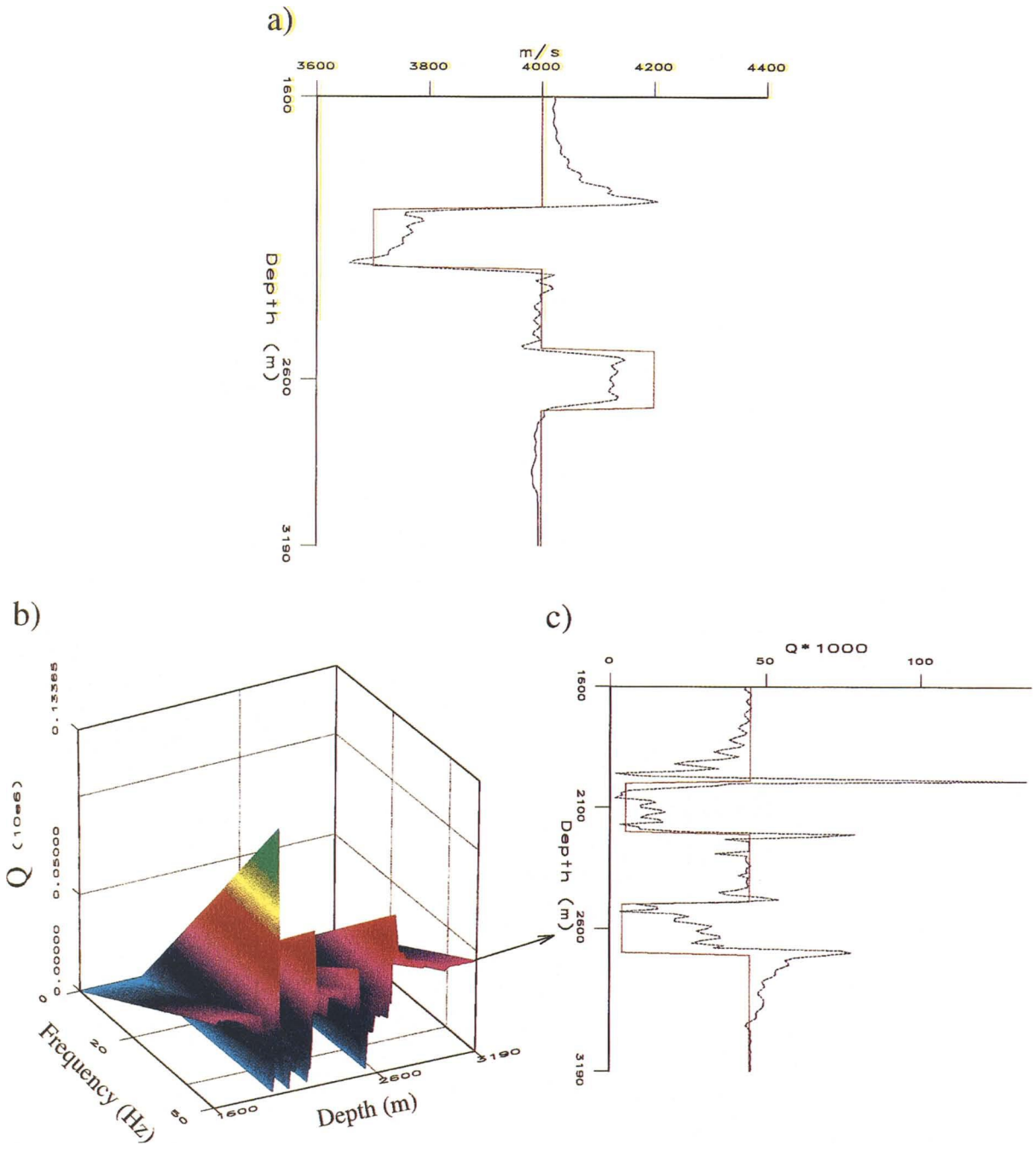

FIG. 5. Recovered medium shown as profiles of the global velocity in (a), and the global quality factor in (c). In (b), the recovered quality factor is plotted for each frequency. The block diagram explicitly shows the linear frequency dependence of the considered Q factor. In (c), the true model is superimposed with the recovered profile at 50 Hz. The continuous line (red) is the true model, the dotted line (black) is the recovered model.

This defocusing comes from the first Born approximation, that uses the Green's function in the background medium even for points inside the attenuating layers. We should specify in the algorithm a reference medium that contains smooth variations of parameters we want to image. The data residuals show a good fit between the observed and synthetic seismograms: only discretization model mesh effects appear.

Noise sensitivity is an indicator of the robustness of the method for attenuation estimation. Observed computed data in Figure 7 are deduced from the observed data in Figure 6 with 10% Gaussian noise-to-signal ratio, band limited to the bandwidth of the data. The recovered profiles are plotted in Figure 4. We note a stability of the recovered profiles for the density and the elastic shear modulus. An accurate position of the medium discontinuities still appears. In presence of noisy data, the recovered attenuation presents more fluctuations, in particular near the second interface. These fluctuations can be related to the influence of the seismogram's amplitude on attenuation imaging. Nevertheless, the profile is still recovered. The small amplitude of the residuals in Figure 7 shows a good fit of the seismograms.

For a better understanding of the convergence process, the misfit function in equation (15) is analyzed quantitatively in the frequency domain, where we were able to control its variation at low as well as high frequencies during the iterations. In Figure 8, for each selected frequency bandwidth, the misfit f_{obt} is normalized by the initial misfit function f_{ini} in this bandwidth; f_{obt} is the value of the misfit obtained summing over all frequencies (i.e., 0.2–50 Hz). We calculate the variance of the error reduction, and we represent a percentage defined as $f_{obt}/f_{ini} \times 100$. We found a decrease of 20%, 60%, and 90%, respectively, in the three selected bandwidths of 0.2–5 Hz,

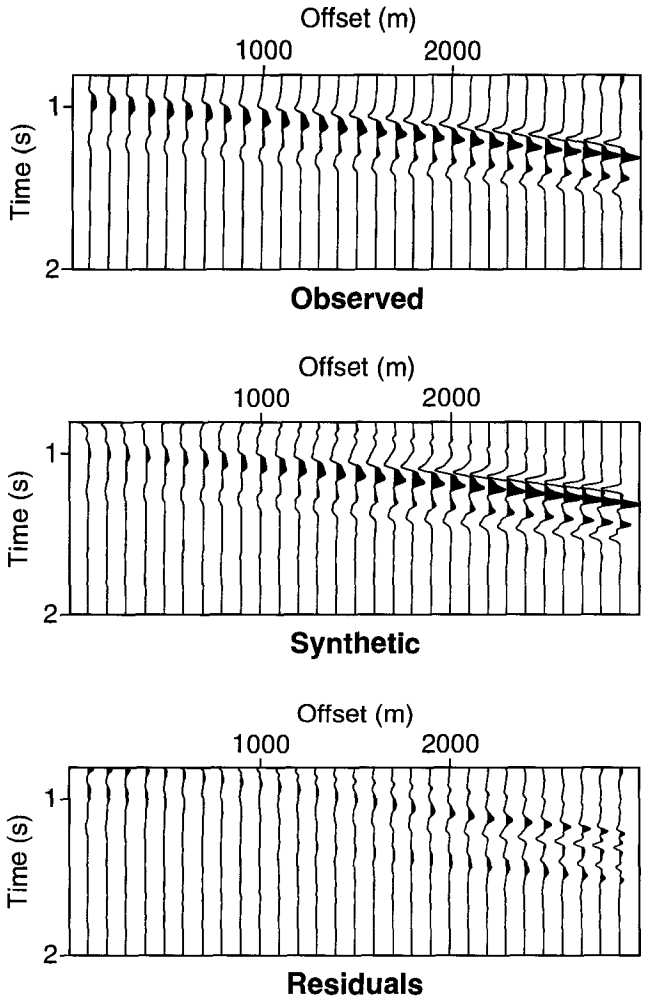

FIG. 6. Synthetic seismograms, obtained by the reflectivity method, are used as observed data (top panel). The offsets correspond to 29 receiver locations. Note the reflection from the top of the first thin layer and from top of the second layer. At zero offset, the reflection starts at 1 s (two-way traveltime) because the top of the first layer is at 2000 m below the surface and the velocity in the background medium is 4000 m/s. The second reflector is detected at 1.24 s. The middle panel shows the synthetic seismograms obtained by Ray-Born approximation for the recovered model; the bottom panel shows the residuals. From the fit between the observed and predicted seismograms and the small amplitude of the residuals, it follows that the recovered model is a good fit of the true model, which shows the convergence of the procedure.

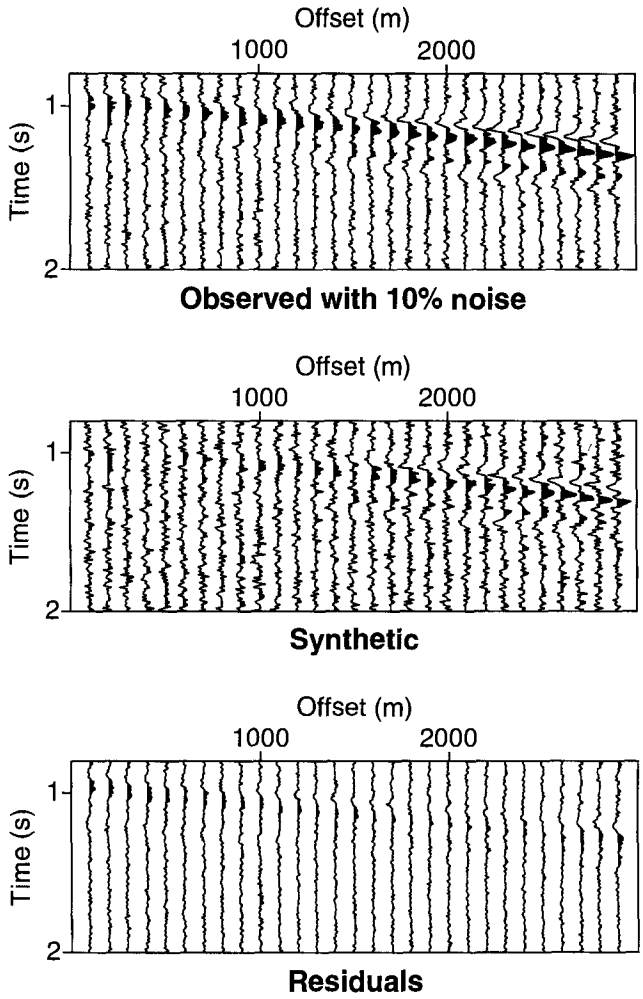

FIG. 7. Noisy synthetic seismograms, corrupted by Gaussian noise band limited to the same frequency as the data, are used as the observed data (top panel). The offsets correspond to 29 receiver locations. The middle panel shows the synthetic seismograms obtained by Ray-Born approximation for the recovered model. On the bottom, residuals have a small amplitude, which proves the convergence of the procedure.

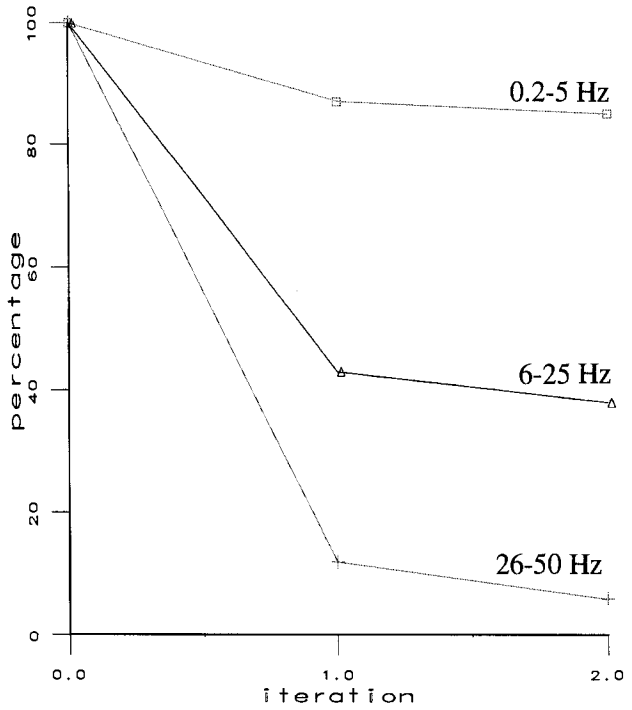

FIG. 8. The percentage of the misfit function for each selected frequency bandwidth.

6–25 Hz, and 26–50 Hz. The fit increases with frequency. We conclude that the approximation of the Hessian expressed in the equation (22) is accurate enough.

Influence of data misfits and model representation recovering in the model space

In most geophysical inverse problems, it is difficult to apply the maximum likelihood method. Consequently, estimation of model parameters errors has usually been performed in an empirical way. Bootstrap statistics involve essentially a resampling technique for estimating errors in the model space (Efron and Tibshirani, 1993). We use a variant of bootstrapping proposed by Nishizawa and Noro (1995). One of the residuals x_k is selected randomly from $X = (x_1, x_2, \ldots, x_n)$ and is added to the kth calculated seismogram u_k^{cal}. We generate a new data set (the bootstrap sample) $\mathbf{u}^\star = (u_1^\star, u_2^\star, \ldots, u_n^\star)$, where $u_k^\star = u_k^{cal} + x_k$. By inserting the bootstrap sample $\mathbf{u}^\star$ in our inversion algorithm, we obtain the residuals associated with the bootstrap sample, $x_i^\star = u_i^\star - u_i^{cal\star}$, and the model parameter $\mathbf{f}^\star$ is reconstructed from the bootstrap data $\mathbf{u}^\star$ in exactly the same way as in the original inversion method.

Applying many "bootstrap" procedures, we obtain many model parameter estimates and, from this empirical distribution, we can calculate the average parameter perturbations, standard deviations, and uncertainties for each parameter. We apply this technique to the example above to evaluate uncertainties in the model parameters because of our inability to explain these residuals; this is not an a posteriori covariance matrix estimation because we do not take into account data errors, for example. The bootstrapping we use is a tool to assess where we should expect good accuracy from our model description and inversion algorithm.

The bootstrap procedure may lead us to overestimate our accuracy when the inverse problem is underdetermined. If a model parameter is weakly constrained by the data, any bootstrapping perturbation in the data space will not affect the model parameter because of significant damping: this parameter will show an anomalously small uncertainty. We see this anomalous behavior below the 2900-m depth, where we are unable to recover model parameters because this distance corresponds to the length of the data acquisition system. We shall not consider deeper estimations of uncertainties. In Figure 9, the propagation parameters (i.e., density and shear modulus, and the dissipation factor) are shown as two extreme models deduced from the mean model with a standard deviation σ. A good location of the interface boundaries is obtained: parameters show an impulsive increase as we cross the boundary. Note that oscillations occurs before and after layers and are caused by our model discretization grid. The bootstrapping technique is unable to overcome this a priori discretization feature. The magnitude of the dissipation factor, which is sensitive to amplitude, is not well recovered in depth. We might deduce that data acquisition configuration should be more severe for recovering attenuation than propagation parameters.

CONCLUSIONS

We have developed a fast inversion technique based on both the Born approximation and asymptotic Green's functions for recovering elastic and attenuation parameters where SH-waves are recorded along the free surface. We have derived a viscoelastic numerical algorithm in the frequency domain in contrast to other researchers who developed elastic and acoustic inversion algorithms in the time domain. In a synthetic test, we successfully recovered the propagation and attenuation parameters. We recovered separately the model parameters in only a few iterations are recovered separately when the data acquisition geometry had good multiplicity in subsurface coverage and when the diffracting zone was of limited extent (Born approximation limit). Inversion of noisy data shows the robustness of the method to recover attenuation information by complete waveform inversion. We underline the importance of a good reference model in our Ray-Born approach. The bootstrap protocol could be used to estimate uncertainties for each parameter because our inversion is fast.

An extension of the method to different modes of propagation is possible, but it will require further analytical analysis.

ACKNOWLEDGMENTS

We are particularly indebted to Stéphane Operto, Gilles Lambaré, and Pascal Podvin (Centre de Recherche en Géophysique, École des Mines de Paris) for constructive and helpful discussions. We are grateful to Anthony Lomax for his proofreading and comments. We also thank Guust Nolet and Robert L. Nowack for their helpful suggestions. This work was partly funded by European Commission and Norvegian Research Council in the framework of the JOULE II program (Project "Reservoir-Oriented Delineation Technology").

REFERENCES

Beydoun, W., and Mendes, M., 1989, Elastic Ray-Born l2 migration/inversion: Geophys. J. Internat., **97**, 151–160.

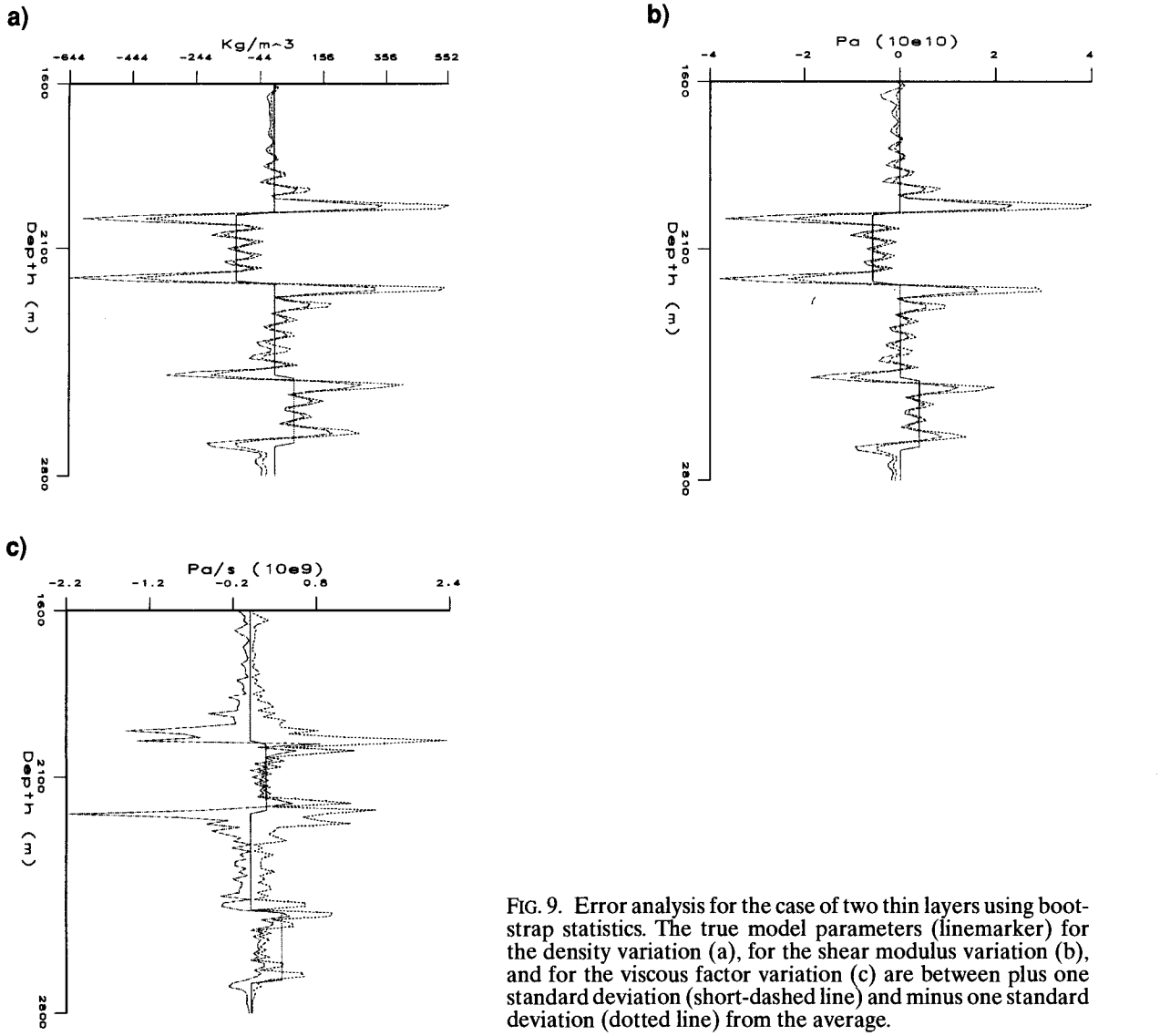

FIG. 9. Error analysis for the case of two thin layers using bootstrap statistics. The true model parameters (linemarker) for the density variation (a), for the shear modulus variation (b), and for the viscous factor variation (c) are between plus one standard deviation (short-dashed line) and minus one standard deviation (dotted line) from the average.

Beylkin, G., 1985, Imaging of discontinuities in the inverse scattering problem by inversion of a causal generalized radon transform: J. Math. Phys., **26**, 99–108.
Beylkin, G., and Burridge, R., 1990, Linearized inverse scattering problems in acoustics and elasticity: Wave Motion, **12**, 15–52.
Bleistein, N., 1984, Mathematical methods for wave phenomena: Academic Press.
——— 1987, On the imaging of reflectors in the earth: Geophysics, **52**, 931–942.
Bourbié, T., 1984, L'atténuation intrinsèque des ondes sismiques, théorie et modèles: Revue de l'Institut Français du Pétrole, **39**, 15–32.
Caviglia, G., Morro, A., and Pagani, E., 1990, Inhomogeneous waves in viscoelastic media: Wave Motion, **12**, 143–159.
Červený, V., and Hron, F., 1980, The ray series method and dynamic ray tracing system for three dimensional inhomogeneous media: Bull. Seis. Soc. Am., **70**, 44–77.
Crase, E., Pica, A., Noble, M., McDonald, J., and Tarantola, A., 1990, Robust elastic nonlinear waveform inversion: Application to real data: Geophysics, **55**, 527–538.
Efron, B., and Tibshirani, R., 1993, An introduction to the bootstrap: Chapman and Hall.
Eringen, A., 1980, Mechanics of continua: Robert E. Krieger Publ. Com.
Fuchs, K., and Müller, G., 1971, Computation of synthetic seismograms with the reflectivity method and comparison with observations: Geophys. J. Roy. Astr. Soc., **23**, 417– 433.
Hearn, D., and Krebes, E., 1990a, Complex rays applied to wave propagation in a viscoelastic medium: Pageoph, **132**, 401–415.
——— 1990b, On computing ray-synthetic seismograms for anelastic media using complex rays: Geophysics, **55**, 422–432.
Hirono, T., 1935a, On the viscoelastic waves (i): J. Met. Soc. Japan, **13**, 413–424.
——— 1935b, On the viscoelastic waves (ii): J. Met. Soc. Japan, **13**, 512–520.
——— 1941, On the viscoelastic waves (iii): Quart. J. Seismol., **11**, 337–348.
Jin, S., Madariaga, R., Virieux, J., and Lambaré, G., 1992, Two-dimensional asymptotic iterative elastic inversion: Geophys. J. Internat., **108**, 1–14.
Lambaré, G., Virieux, J., Jin, S., and Madariaga, R., 1992, Iterative asymptotic inversion in the acoustic approximation: Geophysics, **57**, 1138–1154.
Lee, W., and Solomon, S., 1979, Simultaneous inversion of surface-wave phase velocity and attenuation: Rayleigh and love waves over continental and oceanic paths: Bull. Seis. Soc. Am., **69**, 65–95.
Liu, H., 1995, Application of bandlimited anelastic models to wave propagation in highly attenuative media: Bull. Seis. Soc. Am., **85**, 1359–1372.
Lomitz, C., 1957, Linear dissipation in solids: J. Appl. Phys., **78**, 201–205.
Maxwell, J., 1867, On the dynamical theory of gases: Phil. Trans. Roy. Soc. London, **157**, 49–88.
Miyabe, N., and Ooi, T., 1948, On longitudinal vibration tests: Bull. Seismol. Soc. Japan, **1**, 2–3.
Müller, G., 1983, Rheological properties and velocity dispersion of a medium with power-law dependence of Q on frequency: J. Geophys., **54**, 20–29.
Nishizawa, O., and Noro, H., 1995, Bootstrap statistics for velocity tomography: application of a new information criterion: Geophys. Prosp., **43**, 157–176.

O'Connel, R., and Budiansky, B., 1978, Measures of dissipation in viscoelastic media: Geophys. Res. Lett., **5**, 5–8.
Peltier, W., 1974, The impulse response of a Maxwell earth: Rev. Geophys. Space Phys., **12**, 649–669.
Ribodetti, A., Virieux, J., and Durand, S., 1995, Asymptotic theory for viscoacoustic seismic imaging: 65th Ann. Internat. Mtg., Soc. Expl. Geophys., Expanded Abstracts, 631–634.
Sheriff, R., 1975, Factors affecting seismic amplitudes: Geophys. Prosp., **23**, 125–138.
Tarantola, A., 1986, A strategy for nonlinear inversion of seismic reflection data: Geophysics, **51**, 1893–1903.
——— 1988, Theoretical background for the inversion of seismic waveforms including elasticity and attenuation: Pageoph, **128**, 365–399.
Toksöz, M., and Johnston, D., 1981, Seismic wave attenuation: Soc. Expl. Geophys.
Virieux, J., Flores-Luna, C., and Gibert, D., 1994, Asymptotic theory for diffusive electromagnetic imaging: Geophys. J. Internat., **119**, 857–868.
Voigt, W., 1892, Uber innere reibung fester korper, insbesondere der metalle: Ann. Phys., **47**, 671–693.
White, J., 1965, Seismic waves: Radiation, transmission and attenuation: McGraw-Hill Book Co.
Wu, R., 1989, The perturbation method in elastic wave scattering: Pageoph, **131**, 605–637.

APPENDIX A

FIRST TRANSPORT EQUATION

We solve the first transport equation. We are interested to shear waves. Taking into account $A_0 \cdot \nabla T = 0$, we have

$$-\frac{1}{(\nabla T)^2}[2\mu \nabla T \cdot (\nabla T \cdot \nabla)A_0]\nabla T + (\nabla \mu \cdot \nabla T)A_0 + \mu \Delta T A_0 + 2\mu(\nabla T \cdot \nabla)A_0 + \nu(\nabla T)^2 A_0 = 0. \quad \text{(A-1)}$$

By inner multiplication of equation (A-1) by A_0, we obtain the first transport equation, which governs the evolution of amplitude along the rays:

$$\nabla \cdot [\mu(A_0 \cdot A_0)\nabla T] = -\nu(\nabla T)^2 A_0 \cdot A_0. \quad \text{(A-2)}$$

We can rewrite equation (A-2), describing the energy flux along the raypath, in the form

$$\nabla \cdot (A_0^2 \mathbf{w}) = h A_0^2, \quad \text{(A-3)}$$

where we have imposed $h = -\nu/c^2$, and $\mathbf{w} = \mu \nabla T$.

Following the same procedure as Červený and Hron (1980) and as Caviglia et al. (1990), σ = the arc length along the ray and $w(d/d\sigma) = \mathbf{w} \cdot \nabla$. We calculate

$$\nabla \cdot (A_0^2 \mathbf{w}) = A_0^2(\nabla \cdot \mathbf{w}) + (\mathbf{w} \cdot \nabla)A_0^2. \quad \text{(A-4)}$$

Then

$$A_0^2(\nabla \cdot \mathbf{w}) + (\mathbf{w} \cdot \nabla)A_0^2 = h A_0^2. \quad \text{(A-5)}$$

Consider a point $\mathbf{x}_0$ and a sufficient small surface S_0 that passes through $\mathbf{x}_0$ and is orthogonal to $\mathbf{w}(\mathbf{x}_0)$. Denote by γ_1, γ_2 a pair of parameters which label the rays that pass through S_0. Then, we let the position vector $\mathbf{x}$ at any ray be given by a C^2-function $\mathbf{x} = \mathbf{x}(\sigma, \gamma_1, \gamma_2)$. We consider now the Jacobian J of the mapping via rays as $J = |\mathbf{t}_w \cdot \mathbf{i}_1 \times \mathbf{i}_2|$ (Bleistein, 1984), where $\mathbf{t}_w$ is the unit vector of $\mathbf{w}$, $\mathbf{i}_1 = \partial \mathbf{x}/\partial \gamma_1$, and $\mathbf{i}_2 = \partial \mathbf{x}/\partial \gamma_2$. The generator $\mathbf{w}$ of the flow of rays and J are related by

$$\nabla \cdot \mathbf{w} = w \frac{d \ln(wJ)}{d\sigma}. \quad \text{(A-6)}$$

Then, we can write equation (A-5) as

$$\frac{1}{A_0^2}\frac{dA_0^2}{d\sigma} + \frac{d \ln(wJ)}{d\sigma} = \frac{h}{w}. \quad \text{(A-7)}$$

An integration over σ yields equation (9), the expression of the amplitude.

APPENDIX B

RAY-BORN APPROXIMATION INCLUDING ATTENUATION

In presence of the first-order perturbation of the model parameters in equation (10), the complete Green's function G will be split into the known Green function G_0 and the unknown perturbation δG due to the scattering from the perturbations of model parameters. Then, the local equation (5) for an arbitrary point $\mathbf{x}$ of the medium can be expanded into the following form:

$$\rho_0(\mathbf{x})\omega^2 \delta G(\mathbf{s}, \mathbf{x}, \omega) + \nabla \cdot (\hat{\mu}_0(\mathbf{x}, \omega)\nabla)\delta G(\mathbf{s}, \mathbf{x}, \omega) = -(\omega^2 \delta\rho(\mathbf{x})G(\mathbf{s}, \mathbf{x}, \omega) + \nabla \cdot (\delta\hat{\mu}(\mathbf{x}, \omega)\nabla)G(\mathbf{s}, \mathbf{x}, \omega)). \quad \text{(B-1)}$$

The solution of equation (B-1) can be written as a convolution over the domain $\mathcal{M}$ of diffracting points of the Green's function $G_0(\mathbf{x}, \mathbf{r}, \omega)$, the solution of the equation (6) for the reference medium, with the source term $\omega^2 \delta\rho G + \nabla \cdot (\delta\hat{\mu}\nabla)G$. This, at $\mathbf{r}$, yields

$$\delta G(\mathbf{s}, \mathbf{r}, \omega) = \int_{\mathcal{M}} G_0(\mathbf{x}, \mathbf{r}, \omega)[\delta\rho(\mathbf{x})\omega^2 G(\mathbf{s}, \mathbf{x}, \omega) + \nabla \cdot (\delta\hat{\mu}(\mathbf{x}, \omega)\nabla)G(\mathbf{s}, \mathbf{x}, \omega)]\, d\mathbf{x}. \quad \text{(B-2)}$$

The first-order Born approximation is obtained by replacing the total field G by the incident field G_0 in integral (B-2), leading to the following linear operator between $\delta\rho, \delta\hat{\mu}$, and δG:

$$\delta G(\mathbf{s}, \mathbf{r}, \omega) = \int_{\mathcal{M}} G_0(\mathbf{x}, \mathbf{r}, \omega)\big[\delta\rho(\mathbf{x})\omega^2 G_0(\mathbf{s}, \mathbf{x}, \omega) + \nabla \cdot (\delta\hat{\mu}(\mathbf{x}, \omega)\nabla)G_0(\mathbf{s}, \mathbf{x}, \omega)\big]\, d\mathbf{x}. \quad \text{(B-3)}$$

Integrating the second term on the right hand by parts and noticing that the boundary term vanishes because perturbations $\delta\rho$ and $\delta\hat{\mu}$ are zero on the boundary $\partial\mathcal{M}$ of the domain

$\mathcal{M}$, we obtain the linear relation

$$\delta G(\mathbf{s}, \mathbf{r}, \omega) = \int_{\mathcal{M}} \left[G_0(\mathbf{x}, \mathbf{r}, \omega) G_0(\mathbf{s}, \mathbf{x}, \omega) \delta\rho(\mathbf{x}) \omega^2 - (\delta\hat{\mu}(\mathbf{x}, \omega)\nabla) G_0(\mathbf{x}, \mathbf{r}, \omega) \cdot \nabla G_0(\mathbf{s}, \mathbf{x}, \omega) \right] d\mathbf{x}. \quad \text{(B-4)}$$

Note that the Born approximation requires the scattering zone to have a weak amplitude and a small extension (Wu, 1989).

Moreover, coefficients of the diffracting zone are complex and frequency dependent, which is an added complication with respect to the pure elastic case, i.e., $\delta\hat{\mu}(\mathbf{x}, \omega) = \delta\mu(\mathbf{x}) + i\delta\nu(\mathbf{x})/\omega$. Using asymptotic expressions for Green's functions given by equation (7) and by properties of the perturbation region, the leading asymptotic term of the scattered integral is

$$\delta G(\mathbf{s}, \mathbf{r}, \omega) = \omega^2 \int_{\mathcal{M}} A_0(\mathbf{s}, \mathbf{x}) A_0(\mathbf{x}, \mathbf{r})\, e^{i\omega[T(\mathbf{s},\mathbf{x}) + T(\mathbf{x},\mathbf{r})]} \times e^{-\omega[\alpha(\mathbf{s},\mathbf{x},\omega) + \alpha(\mathbf{x},\mathbf{r},\omega)]} \underset{\sim}{\mathbf{K}} \underset{\sim}{\mathbf{W}} \begin{bmatrix} \delta\rho(\mathbf{x}) \\ \delta\mu(\mathbf{x}) \\ \delta\nu(\mathbf{x}) \end{bmatrix} d\mathbf{x}, \quad \text{(B-5)}$$

where $\underset{\sim}{\mathbf{K}}$ is defined by $(1, 1, i/\omega)$, deduced from the specific Maxwell rheology we have assumed, and the matrix $\underset{\sim}{\mathbf{W}}$ is the Born-scattering matrix previously described.

The physical interpretation of equation (B-5) can be described in the following way. A diffracting point $\mathbf{x}$ reacts to the wave arriving from the source and emits a diffracted wave. This diffracted field recorded at the receiver in Figure 2 is proportional to the amplitude of perturbations of the medium parameters through equation (B-5).

If we define

$$T(\mathbf{s}, \mathbf{x}, \mathbf{r}) = T(\mathbf{s}, \mathbf{x}) + T(\mathbf{x}, \mathbf{r}) \quad \text{and}$$

$$A_0(\mathbf{s}, \mathbf{x}, \mathbf{r}) = A_0(\mathbf{s}, \mathbf{x}) \cdot A_0(\mathbf{x}, \mathbf{r})$$

as quantities related to wave propagation, in particular $T(\mathbf{s}, \mathbf{x}, \mathbf{r})$ is the total traveltime and $A_0(\mathbf{s}, \mathbf{x}, \mathbf{r})$ is the total amplitude. Then we define

$$\alpha(\mathbf{s}, \mathbf{x}, \mathbf{r}, \omega) = \alpha(\mathbf{s}, \mathbf{x}, \omega) + \alpha(\mathbf{x}, \mathbf{r}, \omega),$$

with

$$\alpha(\mathbf{s}, \mathbf{x}, \omega) = \int_{\sigma(\mathbf{s})}^{\sigma(\mathbf{x})} \frac{\nu_0(\xi)}{2c_0(\xi)\mu_0(\xi)\omega}\, d\xi \quad \text{and}$$

$$\alpha(\mathbf{x}, \mathbf{r}, \omega) = \int_{\sigma(\mathbf{x})}^{\sigma(\mathbf{r})} \frac{\nu_0(\xi)}{2c_0(\xi)\mu_0(\xi)\omega}\, d\xi,$$

as the quantities related to total attenuation, finally we obtain the linear relation between the observed data and the perturbation of the model parameters:

$$\delta G(\mathbf{s}, \mathbf{r}, \omega) = \omega^2 \int_{\mathcal{M}} A_0(\mathbf{s}, \mathbf{x}, \mathbf{r})\, e^{i\omega T(\mathbf{s},\mathbf{x},\mathbf{r})}\, e^{-\omega\alpha(\mathbf{s},\mathbf{x},\mathbf{r},\omega)} \times \underset{\sim}{\mathbf{K}} \underset{\sim}{\mathbf{W}} \mathbf{f}(\mathbf{x})\, d\mathbf{x}. \quad \text{(B-6)}$$